ADVANCED FUNCTIONAL MATERIALS
www.afm-journal.de

Materials Views
www.MaterialsViews.com

Layered $LaSrGa_3O_7$-Based Oxide-Ion Conductors: Cooperative Transport Mechanisms and Flexible Structures

By *Cristina Tealdi, Piercarlo Mustarelli,* and *M. Saiful Islam**

Novel melilite-type gallium-oxides are attracting attention as promising new oxide-ion conductors with potential use in clean energy devices such as solid oxide fuel cells. Here, an atomic-scale investigation of the $LaSrGa_3O_7$-based system using advanced simulation techniques provides valuable insights into the defect chemistry and oxide ion conduction mechanisms, and includes comparison with the available experimental data. The simulation model reproduces the observed complex structure composed of layers of corner-sharing GaO_4 tetrahedra. A major finding is the first indication that oxide-ion conduction in $La_{1.54}Sr_{0.46}Ga_3O_{7.27}$ occurs through an interstitialcy or cooperative-type mechanism involving the concerted knock-on motion of interstitial and lattice oxide ions. A key feature for the transport mechanism and high ionic conductivity is the intrinsic flexibility of the structure, which allows considerable local relaxation and changes in Ga coordination.

1. Introduction

A range of energy conversion technologies are being investigated to help cut carbon emissions. In particular, the high efficiency of solid oxide fuel cells (SOFCs) and their fuel flexibility make them viable candidates for distributed cogeneration. These devices require materials that exhibit good oxide-ion conductivity, the optimization of which requires fundamental understanding of ionic transport behaviour.

Research in the area of oxide-ion conductors has concentrated primarily on fluorite-type oxides (such as Y-doped ZrO_2 or Gd-doped CeO_2), and perovskite-type oxides (such as doped $LaGaO_3$), in which oxygen transport proceeds through conventional hopping between oxygen vacancy defects.[1–6] However, there is growing interest in developing alternative electrolytes with lower operating temperatures (600–700°C).[6,7] In particular, novel compounds showing high oxide-ion conductivity, such as apatite-structured $La_{9.33+x}Si_6O_{26+3x/2}$,[8–11] as well as structures containing tetrahedral moieties that include the gallate $La_{1-x}Ba_{1+x}GaO_{4-x/2}$,[12] have been attracting considerable attention.

More recently, layered gallium oxides based on the melilite structure have been proposed as alternative solid electrolyte materials following the exciting discovery of interstitial oxide-ion conductivity in the $LaSrGa_3O_7$-based system,[13] which followed earlier reports concerning transport properties and cation solubility within the melilite structure.[14–16] This compound becomes an interstitial oxide ion conductor when excess oxygen is introduced within the structure by modifying the cation stoichiometry to $La_{1+x}Sr_{1-x}Ga_3O_{7+\delta}$, where $x \approx 0.5$. In particular, ionic conductivity values of 0.02 to 0.1 Scm^{-1} are obtained in the temperature range 600 to 900°C for $La_{1.54}Sr_{0.46}Ga_3O_{7.27}$.[13]

A major puzzle is what is the atomic-scale mechanism controlling oxide-ion transport in this new compound? Based on structural and geometrical considerations, possible interstitial migration paths have been proposed.[13] However, the majority of diffusion or conductivity experiments have encountered difficulties in identifying the atomistic mechanisms controlling ionic transport in this system and other complex oxides. Such mechanistic detail is crucial to gain a greater understanding of the macroscopic transport behavior that underpins potential strategies for optimizing the conductivity, as well as designing next-generation materials.

Here, we combine atomistic (energy minimization) and molecular dynamics (MD) simulation techniques to probe, for the first time, the defect chemistry and oxide-ion migration mechanisms in these new melilite oxide-ion conductors. In particular, the results obtained from long time-scale MD provide new insights into the mechanistic features of interstitial oxygen transport. Atomistic modeling techniques are well suited to the investigation of such properties and have been applied successfully to a variety of studies on ionic or mixed conductors.[10,12,17–21]

2. Results and Discussion

2.1. Structural Modeling

The melilite crystal structure has tetragonal symmetry and is composed of layers of corner-sharing GaO_4 units which are linked to form distorted pentagonal rings (**Figure 1a**). Along the *c* axis, La and Sr are positioned between GaO_4 layers, aligned

[*] Prof. M. S. Islam
Department of Chemistry
University of Bath
Bath, BA2 7AY (UK)
E-mail: m.s.islam@bath.ac.uk
Dr. C. Tealdi, Prof. P. Mustarelli
Dipartimento di Chimica Fisica
Università di Pavia
Viale Taramelli 16, 27100 Pavia (Italy)

DOI: 10.1002/adfm.201001137

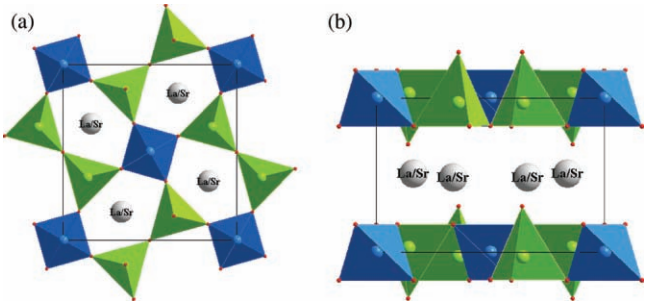

Figure 1. Melilite structure of $LaSrGa_3O_7$: a) view along the *c* axis, showing the Ga tetrahedral units connected through bridging oxygens to form distorted pentagonal rings; b) view along the *b* axis, showing the layered nature of the structure with non-bridging oxygens pointing towards the La/Sr layer. Key: Ga1 (blue); Ga2 (green); O (red); La/Sr (grey).

with the centers of the pentagonal rings (Figure 1b). Neutron diffraction data[13] suggest that the excess oxygen introduced within the structure is positioned within the pentagonal rings, at approximately the same level as Ga.

Two distinct crystallographic sites are occupied by the Ga atoms (labeled Ga1 and Ga2), both in tetrahedral coordination, and three distinct crystallographic sites are occupied by the O atoms. The peculiarity of the $Ga2O_4$ units is the presence of non-bridging oxygen atoms, that is, oxygens that are not shared between Ga units.

The starting point of the study was to reproduce the experimentally observed crystal structures. The experimental crystal structures of the stoichiometric parent compound[22] and the oxygen excess[13] compound were used as the initial structures for modeling. Interatomic potentials and shell model parameters were transferred from previous work,[12,23] with the $Ga^{3+\cdots}O^{2-}$ potential parameters modified slightly for better simultaneous reproduction of the crystal structures of $LaSrGa_3O_7$ and $La_{1.54}Sr_{0.46}Ga_3O_{7.27}$. The final set of interatomic potential and shell model parameters used is presented as Supporting information (Table SI-1) and the corresponding calculated and experimental structures are given in **Table 1**. This table shows that our set of potentials is effective in reproducing the relatively complex crystal structures of both the stoichiometric[22] and overstoichiometric[13] compounds, to within 0.07 Å of the experimental lattice parameters and bond lengths. In particular, the Ga1 and Ga2 environments were well reproduced, which is a non-trivial task. This simulation model therefore provides a valid starting point for the subsequent defect calculations.

2.2. Defect Chemistry and Local Structure

Calculations on intrinsic defects in the parent $LaSrGa_3O_7$ system were performed on the optimized structure. By combining appropriate vacancy and interstitial energy terms, the energies of Frenkel and Schottky defect formation were calculated; the corresponding defect reactions and total energies are given in **Table 2**.

The high energies found for these processes suggest limited concentrations of either Schottky or Frenkel defects in this system. This is in agreement with experimental evidence

Table 1. Experimental and calculated structural parameters a) $LaSrGa_3O_7$; b) $La_{1.54}Sr_{0.46}Ga_3O_{7.27}$ (space group $P42_1m$).

a)	Parameter [Å]	Experimental [33]	Calculated	Δ(Experimental–Calculated)
	a	8.050	8.042	0.007
	c	5.331	5.396	–0.065
	Ga1-O3 (x 4)	1.837	1.804	0.033
	Ga2-O1	1.828	1.801	0.027
	Ga2-O2	1.806	1.781	0.025
	Ga2-O3 (x 2)	1.806	1.811	–0.005

b)	Parameter [Å]	Experimental [13]	Calculated	Δ(Experimental–Calculated)
	a	8.045	7.995	0.050
	c	5.278	5.309	–0.031
	Ga1-O3 (x 4)	1.832	1.813	0.019
	Ga2-O1	1.828	1.802	0.026
	Ga2-O2	1.801	1.789	0.012
	Ga2-O3 (x 2)	1.872	1.829	0.043
	Ga2-O4	2.132	2.146	–0.014

of negligible conductivity and intrinsic disorder in the stoichiometric compound. It is known, however, that concentrations of defects can be introduced into this system by varying the La/Sr ratio, which can be represented by the following equations:

$$La_2O_3 + 2Sr_{Sr}^{\times} \rightarrow 2La_{Sr}^{\cdot} + O_i'' + 2SrO \quad (1)$$

$$2SrO + 2La_{La}^{\times} + O_O^{\times} \rightarrow 2Sr_{La}' + V_O^{\cdot\cdot} + La_2O_3 \quad (2)$$

where $La_{Sr}^{\cdot}$ denotes La on a Sr site with effective +1 charge. The calculated energies for reactions 1 and 2 are 2.67 and 3.15 eV, respectively. Both processes are therefore predicted to be more favorable than the formation of any intrinsic defect listed in Table 2. A preference towards La overstoichiometry (Equation 1) accompanied by formation of O interstitials is found, in good accord with synthesis experiments.[13] As in previous studies, entropic terms are omitted since they are found to be negligible in examining trends in defect formation.

Table 2. Calculated energies of Frenkel and Schottky defects in $LaSrGa_3O_7$.

Defect type	Equation [a]	Energy [eV]
O Frenkel	$O_O^{\times} \rightarrow O_i'' + V_O^{\cdot\cdot}$	4.76
La Frenkel	$La_{La}^{\times} \rightarrow La_i^{\cdot\cdot\cdot} + V_{La}''''$	9.44
Sr Frenkel	$Sr_{La}^{\times} \rightarrow Sr_i^{\cdot\cdot} + V_{Sr}''$	6.54
Ga Frenkel	$Ga_{Ga}^{\times} \rightarrow Ga_i^{\cdot\cdot\cdot} + V_{Ga}'''$	11.52
Full Schottky	$La_{La}^{\times} + Sr_{Sr}^{\times} + Ga_{Ga}^{\times} + 7O_o^{\times} \rightarrow V_{La}'''' + V_{Sr}'' + 3V_{Ga}''' + 7V_o^{\cdot\cdot} + La\,Sr\,Ga_3\,O_7$	58.36

[a] Kroger-Vink notation is used where, for example, $O_O^{\times}$, O_i'', and $V_O^{\cdot\cdot}$ denote an oxygen anion at a regular lattice site, an oxygen interstitial with effective –2 charge, and an oxygen vacancy with effective +2 charge, respectively.

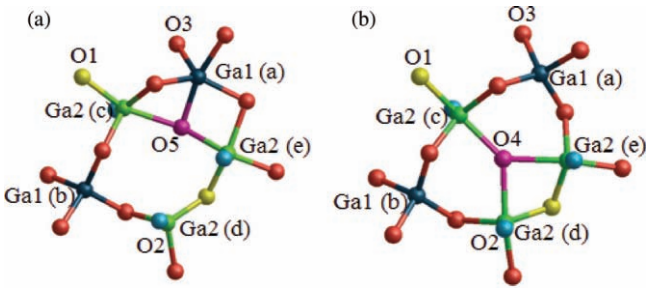

Figure 2. Local relaxation around oxygen interstitials: a) O5 position. b) O4 position. Labels (a) to (e) indicate the Ga sites for the Ga-O distances in Table 3.

Table 3. Ga-O distances and mean local displacements around interstitial oxygen ions after relaxation (Figure 2) [a].

Ga site	Ga-O5 [Å]	Δ [Å]	Ga-O4 [Å]	Δ [Å]
(a)	1.921	–0.017	3.093	+0.039
(b)	4.014	–0.072	3.098	+0.044
(c)	2.138	+0.098	2.048	–0.308
(d)	3.406	–0.042	2.144	–0.222
(e)	1.941	–0.195	2.126	–0.240

[a] Displacements, Δ, are taken as the difference between the final relaxed and the initial unrelaxed distance, and negative values correspond to a shortening of the interatomic distance.

Several possible sites within the pentagonal ring in the Ga layer were considered for the oxygen interstitial, based on those reported by Kuang et al.[13] Our model predicts that the most favorable interstitial position (which we label O5) lies close to (0.42, 0.28, –0.09), slightly off-centered with respect to the gallate channel shown in Figure 1a. The difference in energy between an interstitial at position O5 and one at the center of the pentagonal ring shown in **Figure 2** (labeled O4 by Kuang et al[13]) is 0.66 eV, suggesting that the center of the ring is not the most energetically favorable interstitial site.

A key finding is that considerable lattice ion relaxation occurs around both these interstitial positions. Figure 2b shows that upon relaxation the O4 interstitial tends to become part of the Ga2 environment, changing the coordination of the Ga ion from 4 to 5 as previously suggested.[13] In contrast, Figure 2a shows that upon relaxation the O5 interstitial becomes part of both Ga1 and Ga2 environments (with the Ga1-O5 distance the shorter of the two).

Table 3 reports the final Ga-O distances and mean local displacements for these O4 and O5 interstitials. Analysis of these Ga-O distances around the O5 oxygen interstitial position reveals that at least two of the Ga-O5 bond lengths are shorter than 2.0 Å (namely, Ga ions labeled (a) and (e) in Figure 2); these are close to the values found in the original GaO_4 units (Ga–O1, Ga–O2, Ga–O3 bond lengths in Table 1). It is also clear from Table 2 that the O5 interstitial results in shorter Ga-O distances than the O4 interstitial. This may explain why the O5 site is more energetically favorable than the O4 site, since the O5 interstitial is accommodated by considerable local relaxation of neighboring Ga ions, resulting in the creation of 5-coordinated Ga ions (labeled (a) and (e) in Figure 2).

As suggested by Kuang et al.,[13] the Ga2 ion tends to move closer to the O4 interstitial, with the Ga2-O4 distance opposite to O1 being the shortest, although our calculations indicate that none of the Ga-O4 distances are less than 2 Å.

We stress that to verify that these interstitial energy results were not an artifact of the interatomic potentials chosen, the same calculations were performed using a different set of potentials, characterized by a very different O···O interaction.[24] Even using a different potential set to model the structure, the O5 position was still found to be the most favorable, with an energy difference of approximately 0.5 eV compared to O4. (Details are given as Supporting Information in Table SI-3 to Table SI-5) These results suggest the need for further structural work (e.g., neutron diffraction, pair distribution function (PDF) analysis, NMR spectroscopy) to examine the oxygen defect sites, although we recognize that analysis of such local distortions will not be straightforward.

2.3. Oxygen Migration Mechanisms

Of primary interest here is information on the atomistic mechanism of oxide-ion conduction, which is difficult to extract from experiment alone. We have found that the most favorable oxygen interstitial site (assigned O5) is located off-center within the pentagonal ring. Due to the symmetry of the system, two equivalent O5 interstitial positions exist within the pentagonal ring, as illustrated in **Figure 3a**. We note that this representation does not show the local relaxation around defects and assumes partial occupancy of the oxygen interstitial positions. Our calculations confirm that double occupancy of the same pentagonal ring is highly unfavorable by over 4 eV.

Figure 3a shows that a distinction needs to be made between intra-ring migration and inter- ring migration. Using energy minimization methods, we calculated the energy profile corresponding to the intra-ring migration pathway labeled as A in Figure 3a. In this way, the energy maximum or "saddle-point" configuration was identified, from which the migration energy was derived. The merit of our simulation approach is that it models local lattice relaxation around the migrating oxygen ion and, therefore, the gallate structure is not treated simply as a hard-sphere lattice of fixed ions. Not surprisingly, we find that the saddle point for this migration path is close to the O4 position. Indeed, this energy profile indicates that the O4 interstitial position is actually a local energy minimum, but just below the saddle point (Figure 3b). The calculated activation energy of 0.70 eV for this intra-ring migration is comparable to the value of 0.85 eV measured for the $La_{1.54}Sr_{0.46}Ga_3O_{7.27}$ composition.[13]

Initial results from energy minimization calculations suggest that complex cooperative mechanisms could be the basis of ion migration within the $La_{1.54}Sr_{0.46}Ga_3O_{7.27}$ system (Figure SI-1 and Figure SI-12 in Supporting Information). To investigate these mechanisms in more detail, molecular dynamics (MD) calculations over long simulation time scales were carried out. Such techniques are well suited to probing transport mechanisms directly (especially complex correlated ion motion[25]).

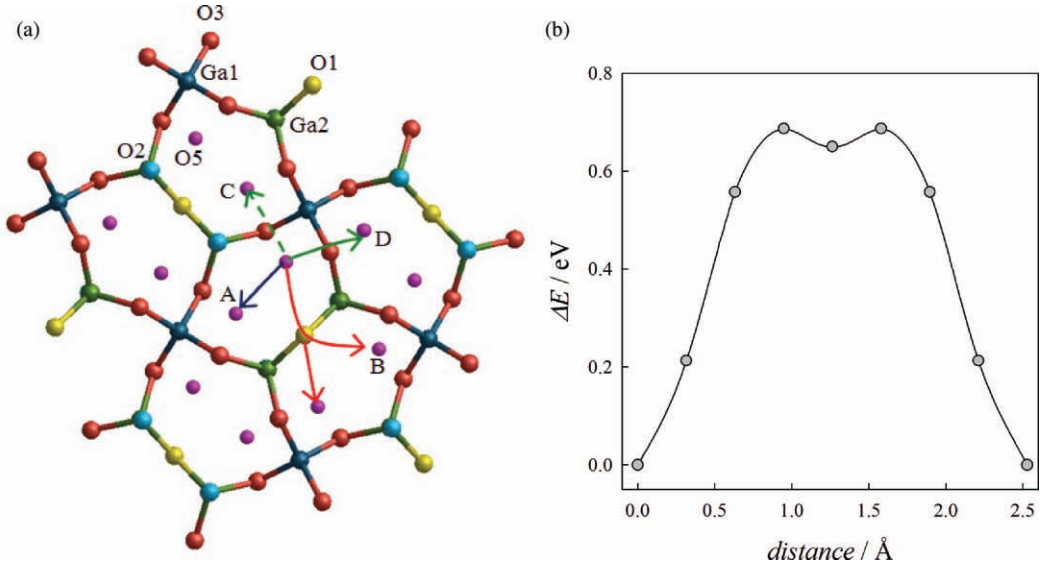

Figure 3. a) Possible intra- and inter-ring paths for oxygen interstitial migration via the most favorable interstitial positions (O5). b) Energy profile for oxygen migration within a pentagonal ring between O5 positions via the O4 position (path A).

First, scatter plots of ion coordinates over the simulated time scale enables the migration paths to be visualized. **Figure 4a** shows neighboring GaO_4, La/Sr and GaO_4-based layers from a projection down the *a* axis. This figure shows that oxide-ion migration within this system is highly anisotropic, restricted exclusively to within the layers of corner-sharing GaO_4 tetrahedra, with no evidence of ion diffusion between adjacent layers. These results confirm that the presence of the large La/Sr cations between GaO_4 layers in the voids bounded by pentagonal rings limits the possibility of oxide-ion migration along the *c* axis.

Figure 4b shows a La/Sr layer viewed perpendicular to the *c* axis. This figure clearly indicates small vibrations of the cations about their lattice sites and typical behavior of an ordered crystalline solid, but with no evidence of ion diffusion; this again suggests that there is no oxide-ion diffusion between adjacent Ga layers.

Figure 5 shows scatter plots of ion positions for two different GaO_4 layers: first, a layer without oxygen interstitials, and second, a layer with a high concentration of oxygen interstitials. Figure 5a shows that when no oxygen interstitials are present within the *ab* plane no long-range diffusion of oxygen ions occurs. Comparison of the shape and size of the positional densities obtained from the scatter plots, particularly for the oxide ions, with those of the thermal ellipsoids from neutron diffraction[13]

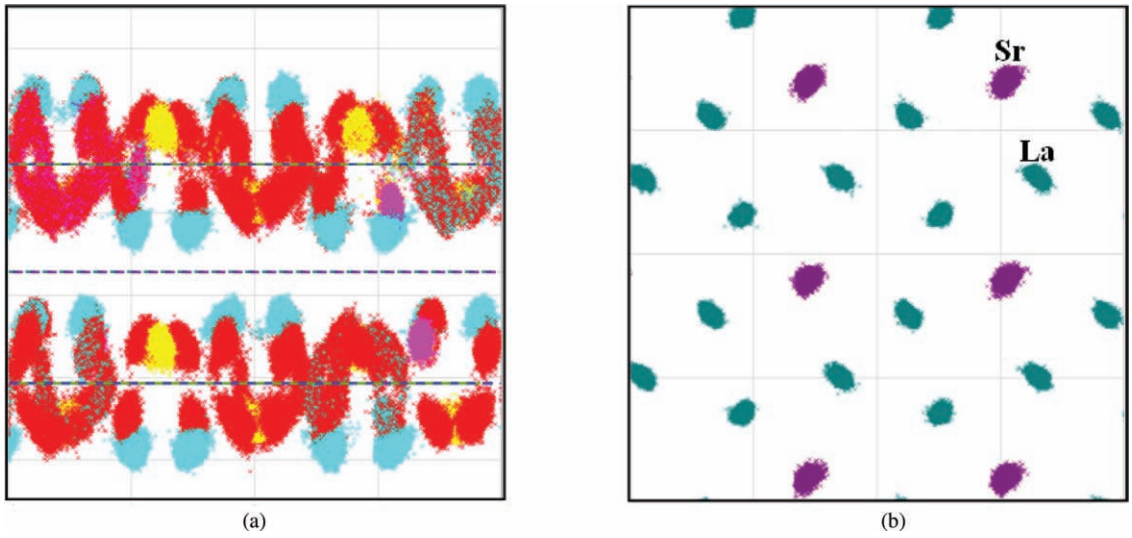

Figure 4. a) Scatter plot of oxide ion positions for $La_{1.50}Sr_{0.50}Ga_3O_{7.25}$ from an MD run in two neighboring Ga layers viewed down the *a* axis. Dotted horizontal lines show the level of the average cation positions on the *z* axis and indicate three adjacent layers: Ga; La/Sr; Ga. Key: (oxygen interstitial (pink), O1 (yellow), O2 (pale blue), O3 (red)). b) Scatter plot of ion positions from an MD run in a La/Sr layer (viewed down the *c* axis) for the $La_{1.50}Sr_{0.50}Ga_3O_{7.25}$ composition. (Green and purple ions are La and Sr respectively).

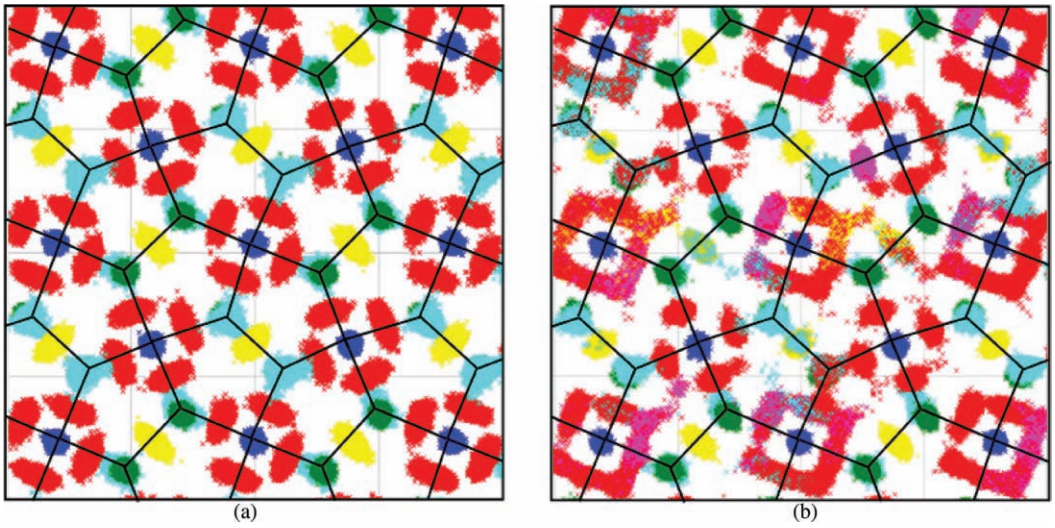

Figure 5. Scatter plot for the $La_{1.50}Sr_{0.50}Ga_3O_{7.25}$ composition from an MD run at 1473 K for 800 ps viewed down the *c* axis; a) layer with no oxygen interstitials, b) layer with a large concentration of oxygen interstitials. Black lines connecting adjacent Ga sites are guides for the eye only. Overlapping of different colors indicates that, over the time scale investigated, oxide ions initially from different crystallographic sites have occupied other sites for varying time spans. Key: yellow (O1); pale blue (O2); red (O3); pink (O5); green (Ga2); blue (Ga1).

shows very good agreement. Another notable feature is that the density of O3 ions is greater than the other oxygen sites; this is a consequence of the rotational motion of the GaO_4 tetrahedral units within the gallate layer.

When oxygen excess is present within the layer (Figure 5b), there is considerable motion of the oxide ions. An important feature is that the diffuse distribution and overlapping of different oxygen positions indicates that numerous different oxide ions are moving between lattice and interstitial sites. This suggests that oxide-ion conduction in this melilite-structured gallate takes place by an "interstitialcy" or "knock-on" mechanism in which the migrating O^{2-} interstitial displaces a lattice ion into a neighboring interstitial position. Such a mechanism has long been believed to dominate F^- interstitial migration in fluorite-related $RbBiF_4$[25] as well as cation migration in Li_3N,[26] but has not been widely elucidated in complex mixed-metal oxides.

For further detailed analysis, in **Figure 6** we have focused, as selected examples, on frequently occurring diffusion events involving intra- and inter-ring oxide-ion migration (equivalent to paths A and B in Figure 3). The scatter plots and migration paths in Figure 6 reveal three main features. First, facile rotation of the GaO5 units occurs, which allows rapid migration of oxide ions via O3 positions (along paths C and D in Figure 3). A key feature for oxide-ion conduction, therefore, is the intrinsic flexibility and dynamical deformation of the structure, as found in the related $LaBaGaO_4$-based ion conductor.[12]

Second, the most favorable interstitial position, corresponding to that occupied for the longest time, is the O5 position, which supports the results of our energy minimization calculations. During long-range diffusion, the O4 position is also occupied to some extent, but the lower density of points about this site suggests that it is a migration transition state and less stable than the O5 position.

Third, all of the oxide ions are involved in the long-range diffusion of oxygen, in which the simulations reveal a high degree of correlation between the motions of different oxygen ions. For example, from analysis of the ion coordinates over the simulation time scale the O1 oxygen moves approximately 4 Å (from the original O1 lattice position to the final O3 lattice position), while the O3 oxygen covers a distance of nearly 8 Å (see Supporting Information Figure SI-3).

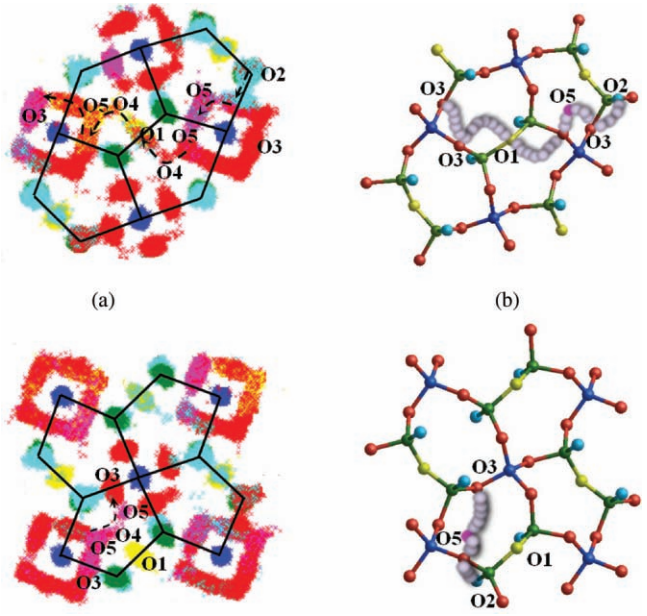

Figure 6. Close-up of oxide-ion migration paths in $La_{1.50}Sr_{0.50}Ga_3O_{7.25}$ a) Migration from O5 to O5 via an O4-O1-O4 linkage; b) Migration from O5 to O5 via an O4 site. Left panel: scatter plot from the MD run at 1473 K for 800 ps; labels indicate the initial crystallographic positions, and solid lines connecting adjacent Ga sites are guides for the eye only; Right panel: schematic representation of the migration paths. Key: Ga1 (blue); Ga2 (green); O (red).

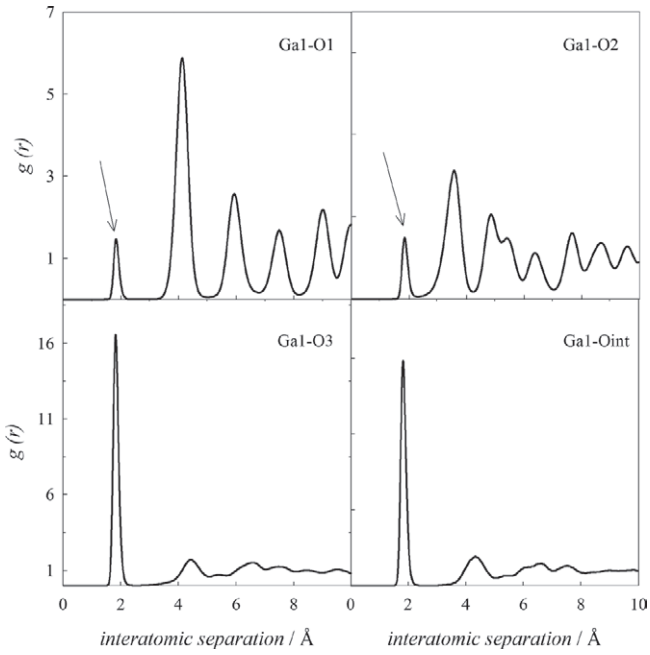

Figure 7. Partial radial distribution functions (RDFs) for Ga1-O interactions. Arrows indicate sharp peaks located at the same distance as for Ga1-O3 (1.8 Å) in the Ga1-O1 and Ga1-O2 RDFs, and show that some ions initially on O1 and O2 sites have migrated onto O3 sites.

Valuable structural information can be gleaned from radial distribution functions (RDFs), which often provide insight into the long-range (dis)order of the material. **Figure 7** shows the partial RDFs for Ga1-O interactions calculated over the simulation time, and indicate two important features. First, the most mobile oxygen species are those originally on the interstitial and O3 sites, shown by their weak, diffuse structures beyond the first coordination shell, indicative of greater disorder.

Second, sharp peaks centered at about 1.8 Å for the Ga1-O1 and Ga1-O2 separations are evident (highlighted in Figure 7 with an arrow). We recall that Figure 2 shows that Ga1 is coordinated by O3 sites only in the initial structure at a distance of approximately 1.8 Å, whereas O1 and O2 sites are coordinated exclusively to Ga2. However, Figure 7 shows that at high temperature and over an extensive simulation time, ions originally on O1 and O2 sites become coordinated to Ga1, with bond lengths identical to those found for Ga1-O3 in the experimental structure.[13] This again indicates that substantial long-range migration of oxide ions has occurred, with ions originally on different sites exchanging positions with other sites throughout the structure during the migration process. Hence, as found from the scatter plot of ion positions, all the oxide ions (O1-O5) are involved in the mechanism for oxide-ion transport within this gallate material.

3. Conclusions

In summary, this atomic-scale investigation has allowed us to gain valuable insights into the defect chemistry and oxide-ion conduction mechanisms in layered gallates based on $La_{1+x}Sr_{1-x}Ga_3O_{7+\delta}$ (x~0.5), which have attracted recent interest as novel oxide-ion conductors for solid oxide fuel cells. Such mechanistic detail is difficult to extract from experiment alone.

Three important features are highlighted. i) The first indication that oxide-ion conduction occurs through an interstitialcy or cooperative-type mechanism involving the concerted knock-on motion of interstitial and lattice oxygens. Such an unusual mechanism has not been widely elucidated in pure oxide-ion conductors. ii) Oxide-ion diffusion is highly anisotropic and restricted to within the layers of corner sharing GaO_4 tetrahedra. iii) Facile rotation of the GaO_5 units facilitates the migration of oxygen interstitials to adjacent pentagonal rings. Indeed, an important feature for this transport mechanism and for good conductivity is the flexibility of the structure, which allows considerable local relaxation and changes in Ga coordination. Such structural flexibility is believed to be crucial for other oxide-ion conductors based on Si/Ge apatites and $LaBaGaO_4$-based materials, which also have tetrahedral units.

These features may be important for the optimization and design of the next generation of fuel cell materials, and warrants further investigation.

4. Experimental Section

Our description of the computational techniques will be brief since detailed reviews are given elsewhere.[27] The two major techniques employed in this study are the static lattice (energy minimization) and molecular dynamics (MD) methods. The GULP code was used for all energy minimization simulations.[28] Interactions between ions were modeled with a Buckingham potential, which account for electron cloud overlap and van der Waals interactions, with electronic polarizability described by the shell model.[29] Lattice relaxation around charged defects is treated using the Mott-Littleton method. MD simulations were performed with the DL_POLY code using an orthogonal simulation box with periodic boundary conditions.[30] The simulation box consisted of $3 \times 3 \times 8$ unit cells, giving a composition of $La_{1.5}Sr_{0.5}Ga_3O_{7.25}$, which contains 36 interstitial oxygen atoms per box, and is close to the experimental composition $La_{1.54}Sr_{0.46}Ga_3O_{7.27}$ that displays high oxide-ion conductivity. The system was equilibrated first under a constant pressure of 1 atm and temperature of 1473 K for at least 120 000 time steps (with a time step of 1 fs). The main simulation run of 800 000 time steps was performed in the NVT ensemble (at $T = 1473$ K) to give a long simulation time of 800 ps. Such large supercells, long time-scales and greater statistics are currently not accessible by ab initio methods.

Supporting Information

Supporting Information is available from the Wiley Online Library or from the author.

Acknowledgements

We are grateful to Dr Craig Fisher (Nagoya, Japan) and Dr Pooja Panchmatia (Bath, UK) for useful discussions. C. T. gratefully acknowledges the Cariplo Foundation for a post-doctoral fellowship. This article was amended October 28, 2010 to correct an error in Table 2.

Received: June 4, 2010
Published online: August 27, 2010

[1] B. C. H. Steele, A. Heinzel, *Nature* **2001**, *414*, 345.
[2] J. B. Goodenough, *Ann. Rev. Mater. Res.* **2003**, *33*, 91.
[3] a) L. Malavasi, C. A. J. Fisher, M. S. Islam, *Chem. Soc. Rev.* **2010**, in press, DOI:10.1039/b915141a; b) V. V. Kharton, F. M. B. Marques, A. Atkinson, *Solid State Ionics* **2004**, *174*, 135; c) S. M. Haile, *Acta Mater.* **2003**, *51*, 5981.
[4] a) S. Tao, J. T. S. Irvine, J. A. Kilner, *Adv. Mater.* **2005**, *17*, 1734; b) J. Januschewsky, M. Ahrens, A. Opitz, F. Kubel, J. Fleig, *Adv. Funct. Mater.* **2009**, *19*, 3151.
[5] L. Malavasi, C. Tealdi, C. Ritter, *Angew. Chemie. Int. Ed.* **2009**, *48*, 8539.
[6] S. J. Skinner, J. A. Kilner, *Mater. Today* **2003**, 30.
[7] a) J. W. Fergus, *J. Power Sources* **2006**, *162*, 30; b) A. Orera, P. R. Slater, *Chem. Mater.* **2010**, *22*, 675.
[8] S. Nakayama, T. Kageyama, H. Aono, Y. Sadaoka, *J. Mater. Chem.* **1995**, *5*, 1801.
[9] L. Leon-Reina, E. R. Losilla, M. Martinez-Lara, S. Bruque, M. A. G. Aranda, *J. Mater. Chem.* **2004**, *14*, 1142.
[10] J. R. Tolchard, M. S. Islam, P. R. Slater, *J. Mater. Chem.* **2003**, *13*, 1956.
[11] E. Kendrick, M. S. Islam, P. R. Slater, *J. Mater. Chem.* **2007**, *17*, 3104.
[12] E. Kendrick, J. Kendrick, K. S. Knight, M. S. Islam, P. R. Slater, *Nat. Mater.* **2007**, *6*, 871.
[13] X. Kuang, M. A. Green, H. Niu, P. Zajdel, C. Dickinson, J. B. Claridge, L. Jantsky, M. J. Rosseinsky, *Nat. Mater.* **2008**, *7*, 498.
[14] M. Rozumek, P. Majewski, L. Sauter, F. Aldinger, *J. Am. Ceram. Soc.* **2004**, *87*, 662.
[15] M. Rozumek, P. Majewski, H. Schluckwerder, F. Aldinger, K. Kunstler, G. Tomandl, *J. Am. Ceram. Soc.* **2004**, *87*, 1795.
[16] E. S. Raj, S. J. Skinner, J. A. Kilner, *Solid State Ionics* **2005**, *176*, 1097.
[17] a) M. S. Islam, *J. Mater. Chem.* **2000**, *10*, 1027; b) M. S. Islam, P. R. Slater, *MRS Bull.* **2009**, *34*, 935.
[18] a) X. X. Guo, J. Maier, *Adv. Funct. Mater.* **2009**, *19*, 96. b) D. Rupasov, A. Chroneos, D. Parfitt, J. A. Kilner, R. W. Grimes, S. Y. Istomin, E. V. Antipov, *Phys. Rev. B* **2009**, *79*, 172102; c) D. Marrocchelli, P. A. Madden, S. T. Norberg, S. Hull, *J. Phys.: Condens. Matter*, **2009**, *21*, 405403;
[19] a) C. A. J. Fisher, M. Yoshiya, Y. Iwamoto, J. Ishii, M. Asanuma, K. Yabuta, *Solid State Ionics* **2007**, *39–40*, 3425; b) T. X. T. Sayle, S. C. Parker, D. C. Sayle, *J. Mater. Chem.* **2006**, *16*, 1067; c) Y. D. Li, T. P. Hutchinson, X. J. Kuang, P. R. Slater, M. R. Johnson, I. R. Evans, *Chem. Mater.* **2009**, *21*, 4661.
[20] a) E. Kendrick, M. S. Islam, P. R. Slater, *Chem. Commun.* **2008**, 715; b) A. Jones, P. R. Slater, M. S. Islam, *Chem. Mater.* **2008**, *20*, 5055.
[21] a) J. R. Tolchard, P. R. Slater, M. S. Islam, *Adv. Funct. Mater.* **2007**, *17*, 2564; b) G. C. Mather, M. S. Islam, F. M. Figueirido F M, *Adv. Funct. Mater.* **2007**, *17*, 905.
[22] J. M. S. Skakle, R. Herd, *Powder Diffr.* **1999**, *14*, 195.
[23] G. V. Lewis, C. R. A. Catlow, *J. Phys. C Solid State Phys.* **1985**, *18*, 1149.
[24] L. Minervini, M. O. Zacate, R. W. Grimes, *Solid State Ionics* **1999**, *116*, 339.
[25] C. R. A. Catlow, R. G. Bell, J. D. Gale, *J. Mater. Chem.* **1994**, *4*, 781.
[26] C. R. A. Catlow, *J. Chem. Soc., Faraday Trans.* **1990**, *86*, 1167.
[27] C. R. A. Catlow, in *Computer Modelling in Inorganic Crystallography*; Academic Press, San Diego **1997**.
[28] J. D. Gale, *J. Chem. Soc., Faraday Trans.* **1997**, *93*, 629.
[29] B. G. Dick, A. W. Overhouser, *Phys. Rev.* **1958**, *112*, 90.
[30] W. Smith, T. R. Forester, *J. Mol. Graphics* **1996**, *14*, 136.